Article

Silica fume improves the frost resistance of alkali-activated slag/fly ash geopolymer binder

Sen Wang, Yuqing Liang, Duosi Mo, Chonghui Zhang, Jiwei Xue, Xuewen Song and Yachao Wang

School of Resources Engineering, Xi'an University of Architecture & Technology, Xi'an, 710055, China
* Correspondence: of the corresponding author: wangyachao@xauat.edu.cn

Abstract: Benign design of alkali-activated slag/FA geopolymer paste has intriguing increasing attention for optimizing its service performance. Therefore, the replacement of fly ash (FA) with 10 wt% silica fume (SF) is investigated by mechanical strength after freeze-thawing cycles and microstructure characterization. The results show that an appropriate dosage (30 wt%) of slag is necessary to attain alkali-activated slag/FA geopolymer paste with excellent mechanical performance, and the SF/slag/FA (SF: slag: FA= 10:30:60, wt%) geopolymer paste exerts the compressive and flexural strength of 95.2 and 3.2 MPa, respectively. Meanwhile, the doped 10 wt% SF facilitates the propagation of (N, C)-A–S–H chains, rather than the formation of C-S-H gels, evidenced by the absent exothermic peak at about 861°C from the differential scanning calorimetry (DSC) curves, leading to the increases in the pores volume with a pore diameter<20 nm and tortuosity by mercury intrusion porosimeter (MIP) results, corresponding to an improved freezing-thawing resistance with the residual compressive strength of 52.8 MPa and the weight loss of 10.5% after 300 freeze-thawing cycles. It explores a cost-effective and benign facile approach to designing heating curing-free alkali-activated slag/FA geopolymer paste with good freezing-thawing resistance.

Keywords: alkali-activated; freezing-thawing; fly ash; geopolymer; silica fume

1. Introduction

Geopolymers have been being currently developed as an environmentally beneficial alternative to Portland cement for concrete production, offering comparable performance and cost-efficient techniques while reducing greenhouse gas emissions [1-2]. Geopolymerization could convert a wide range of metallurgical waste alumino-silicate materials including fly ash (FA), slag, and steel slag into cementitious materials, such as pastes and binders. Nevertheless, the multifunctional design of geopolymer has intriguing increasing attention by adjusting multi-component metallurgical solid wastes [3-5], such as fire protection, thermal stability, and ultra-high toughness, as well as the freezing-thawing resistance.

Meanwhile, previous reports have manifested that slag affects most of the physical and chemical properties of the final product, playing an important role during synthesis and also in determining the long-term durability of alkali-activated slag/FA binders [6-7], noticeable amounts of slag exert a strengthening effect for preparation of FA-based geopolymer cured at room temperature, rather than the heating curing at about 80 °C. Ismail et al. [8] investigate the performance of alkali silicate-activated FA/slag geopolymer binders subjected to sulfate exposure. Because the main products of alkali-activated FA/slag contain hydrotalcite and C-S-H gels, leading to an increase in the total amount of chemical shrinkage [9].

However, the alkali-activated slag/FA binder possesses strong fragility and poor pliability, a lot of methods have been explored to reinforce and toughen the binder [10, 11]. To track this problem with a cost-effective approach, the incorporation of other solid wastes has been intriguing the increasing attention, such as calcium carbide residue and Glauber's salt [12], calcium carbide slag and sodium metasilicate powder [13], salt-loss

 doi:10.20944/preprints202306.0562.v1

soda residue and oxalate acid [14], as well as the waste perlite powder [15]. Therefore, the multicomponent geopolymer consists of various solid wastes and is in full swing to pursue high-performance and multi-function cementitious materials.

Currently, very few studies have taken silica fume (SF) into account for further optimizing the service property of alkali-activated slag/FA binder. Theoretically, SF possesses an amorphous structure and the highest reaction activity due to its lowest binding energy, which has attracted much attention and investigation in the Portland cement system. In the non-sintered cement system, SF-derived activators give reaction products that are very similar to those obtained using commercial silicate solutions, as a consequence of the high reactivity of this precursor, supplying high concentrations of Si to the systems since the early stages of reaction [16]. Jose et al. [17] suggest the optimum silica replacement is 5%–10% and it could serve as heterogeneous nucleation centers for the hydration products after the dissolution of the glassy slag by the alkali-activation. Thus, the mechanical strength of SF-doped alkali-activated slag/FA binder needs to be further clarified to explore low-cost geopolymers with high performance. Additionally, the frost-thawing resistance of alkali-activated binder is also crucial to evaluate its usability [18], especially for the severe-cold region. Because of the coupling effect of internal frost-heave stress induced by phase transition and external frost-heave stress induced by ice contraction [19], the alkali-activated slag/FA binder is vulnerable and fragile to undertake the frost attack. Regarding the SF doped alkali-activated slag/FA binder, the SF could improve the mechanical strength, but the freeze-thaw resistance of the trinary binder needs to be clarified because a higher compressive strength does not necessarily indicate a better freeze–thaw resistance [20].

Consequently, the identification of a strong correlation between FA, slag, and SF in the slag/FA binder studied here is significant in determining whether these materials would meet wide approval in the local market. It is necessary to explore a simple-yet-effective solution for the utilization of industrial solid wastes. The primary purpose of this paper is to address the following questions: based on the optimum slag dosage in alkali-activated slag/FA-based geopolymer, micro-structure evaluation of SF doped slag/FA binder are investigated through the replacement of FA with 10 wt% SF [21]. The mechanical properties, freeze–thaw resistance, pore structure, differential scanning calorimetry (DSC), morphology, and x-ray diffraction (XRD) spectra are studied systematically to clarify the SF'effect on the freeze-thaw resistance of slag/FA geopolymer paste. Generally, it explores a cost-effective and benign facile approach to design heating curing-free alkali-activated slag/FA geopolymer paste with good freezing-thawing resistance, clarifying the reactive priority between the (N, C)-A–S–H chains and the C-S-H gels to construct durable cementitious materials.

2. Materials and characterizations

2.1. Starting materials

FA with a Blaine-specific surface area of 500 m^2/kg and a mean particle size of 11.2 μm after oven drying at 105°C and ball-milling for 1 h was obtained from Hancheng power plant. Granulated ground blast furnace slag (slag) was obtained from Delong powder company with a Blaine-specific surface area of 420 m^2/kg and a mean particle size of 15.5μm. Silica fume (SF) was derived from Linyuan chemical reagent company. The chemical compositions of raw materials were given in **Table 1**. Alkali-activator, $Na_2SiO_3 \cdot 9H_2O$ (A.R.), presented spherical grains with an activator modulus of 1.0, it was purchased from Yaohua chemical reagent company.

Preprints (www.preprints.org) | NOT PEER-REVIEWED | Posted: 7 June 2023 doi:10.20944/preprints202306.0562.v1

Table 1. Chemical compositions of raw materials.

Raw materials	Mass percent (wt %)									
	CaO	SiO_2	Al_2O_3	Fe_2O_3	MgO	Na_2O	K_2O	SO_3	TiO_2	Loss
Fly ash	3.82	55.18	31.19	5.07	0.60	0.29	1.99	0.28	1.05	0.53
Slag	37.65	31.29	14.31	0.61	8.51	0.63	0.58	4.94	0.83	0.54
SF	0.60	87.18	6.89	1.18	0.45	0.28	0.66	0.32	— —	2.11

2.2. Preparation of specimens

The heating curing-free alkali-activated slag/FA geopolymeric binder was synthesized by adding sodium silicate (15wt%, $Na_2SiO_3 \cdot 9H_2O$) solution into the uniform mixture of FA and slag with a water/(slag+FA) ratio of 0.3 to form the slurry in a cement mortar machine, the weight ratio of FA to slag were 80/20, 70/30, and 60/40, respectively, and then poured the slurry into a stainless triplet mold of 160×40×40 mm^3, demoulded after curing for one day in a standard curing box of cement. Finally, the specimens were put into a curing box for another 27d at RT with an 85% relative humidity. Based on the optimum slag dosage in alkali-activated slag/FA geopolymer, the replacement of FA with 10 wt% SF was studied, and therefore the weight ratio of SF: slag: FA was 10:30:60 as the starting materials to prepare the specimen. Freeze-thaw cycles were by ASTM C666, Procedure A, the test was conducted by Hengnai measurement apparatus, one freeze–thaw cycle was carried out in 2–5 h, and the thawing time should not be less than a quarter of the total time of one cycle. At the end of freeze-thawing, the temperature of the specimen center should be controlled at -18℃ and 5°C, respectively.

2.3. Characterizations

Compressive strengths were tested by a full-automatic cement compressive testing machine of YAW-300 type with a pressurization rate of 2.4 kN/s, the testing error was 0.5MPa. Flexural strengths were measured by a motorized bending tester of DKZ-5000 type, the testing error was 0.2MPa. Micro-morphology analysis of samples was conducted on a Quanta 200 scanning electron microscope (SEM) with a working condition of 20kV voltage. Pore size distributions of samples after 28d curing were tested by an AUTOPORE 9500 mercury intrusion porosimeter (MIP) with a tortuosity measurement of the sample under nitrogen pressure of 0.3MPa, the testing error of tortuosity was 2. XRD patterns of specimens were conducted on a D/MAX-2400 X-ray diffractometer equipped with a rotation anode using Cu Kα radiation. Differential scanning calorimetry (DSC) of Mettler tested the heat flow of specimens after 28d curing, it was conducted during the heating process of 50-950℃ under a nitrogen atmosphere at a heating rate of 30℃/min.

3. Results and discussion

3.1. Mechanical properties of specimens

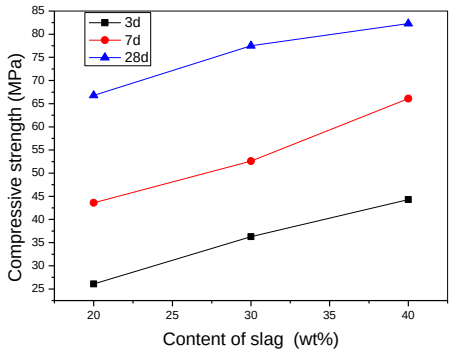

Figure 1. Compressive strength of specimens.

Preprints (www.preprints.org) | NOT PEER-REVIEWED | Posted: 7 June 2023 doi:10.20944/preprints202306.0562.v1

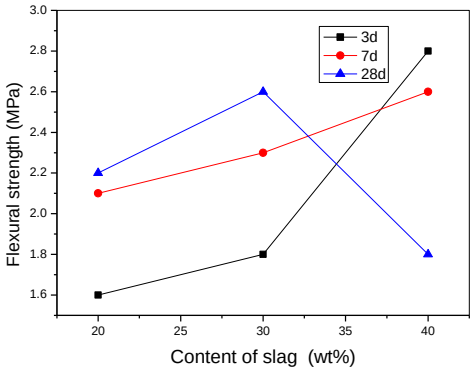

Figure 2. Flexural strength of specimens.

Figure 1 displays the compressive strengths of specimens, which climbs with the increasing dosage of slag, it determines that incorporated slag facilitates a higher cementitious reactivity with a substantial increase in the compressive strength. The 28d compressive strength of the specimen with 40 wt% slag reaches 82.3 MPa while it is 66.8 MPa for the specimen with 20 wt% slag, which reveals that the active calcium derived from slag plays an important role in improving the mechanical performance. It is proposed [14, 22] that the hardening process is initiated by the precipitation of C-S-H/(N, C)-A–S–H gels together, and rapid hardening continues on account of accelerated geopolymerization.

On the contrary, the 28d flexural strength of the specimen with 40 wt% slag decreases sharply after 7d curing as shown in **Figure 2**, it drops to 1.8 MPa while it is 2.6 MPa for the specimen with 30 wt% slag, implying that excess free calcium exerts a reverse effect, to the disadvantage of the flexural strength, due to the interruption of the (N, C)-A–S–H chain gels by the newly-formed C-S-H gels, inhibiting or impeding the chain propagation, thus more interfaces or cracks form and grow, leading to a decrease in flexural strength. As a whole, it determines that there is a critical dosage (30 wt%) of slag content for slag/FA geopolymer paste to attain excellent compressive strength as well as flexural strength.

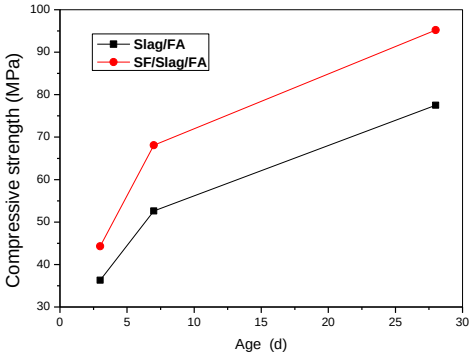

Figure 3. Compressive strength of SF/slag/FA binder.

Preprints (www.preprints.org) | NOT PEER-REVIEWED | Posted: 7 June 2023 doi:10.20944/preprints202306.0562.v1

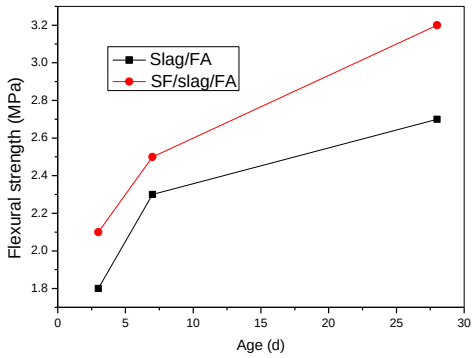

Figure 4. Flexural strength of SF/slag/FA binder.

Meanwhile, the mechanical performance of SF doped slag/FA (SF: slag: FA=10:30:60, wt.%) binder is shown in **Figure 3-4**, using the alkali-activated slag/FA (30:70,wt.%) binder as the reference. The 28d compressive strength is improved to 95.2 MPa (increased by 22.8%) and the flexural strength rises to 3.2 MPa (increased by 23.1%) after replacement of 10 wt% FA with SF. It demonstrates incorporating SF into slag/FA binder is an effective method to alleviate the inherent fragility of alkali-activated slag/FA binder, the more amorphous $Si(OH)_4$) derived from the SF is prone to crosslink with the (N, C)-A–S–H chain, rather than transforms into C-S-H gels, evidenced by the simultaneously increased flexural strength, compared with the reduced flexural strength of sample 40S.

3.2. Pore distributions of specimens

Table 2. Pore size distributions of specimens.

Specimens	<20nm (%)	20-200nm (%)	0.2-3μm (%)	>3μm (%)	Median pore diameter (nm)	Porosity (%)	Tortuosity
20S	0.02	41.18	10.03	48.76	48.2	21.05	12.44
30S	32.25	18.62	7.79	41.34	7.7	19.08	60.37
40S	40.02	9.17	11.39	38.43	6.4	20.93	81.74
30S+10SF	41.16	3.14	35.81	19.88	5.6	13.47	116.9

Note: 20S-incorporating 20 wt% slags into FA, 30S-incorporating 30 wt% slag into FA, 40S-incorporating 40 wt% slags into FA, 30S+10SF-incorporating 30 wt% slag and 10 wt% SF into FA.

The pore size distributions of specimens are summarized in **Table 2**. Combined with the mechanical performance, it is found that the median pore diameter and total porosity are inversely proportional to the compressive strength. The median pore diameter of the specimen drops from 48.2 nm to 6.4 nm with the increasing slag dosage gradually. Meanwhile, the pore volume of pore with a diameter<20 nm increases following the compressive strength. Because the FA is transformed into geopolymerical gels and slag could hydrolyze to active C-H-S and (N, C)-A–S–H sols under an alkaline environment, which could insert and fill into the clearance of cross-linked network derive from the gels, forming a compact microstructure with a lower porosity and the reduced median pore diameter.

Interestingly, the increasing tortuosity matches the improvement of compressive strength value, it reveals that the compact micro-structure holds tortuous pore channels, which are triggered by the filling effect of the amorphous binder. Song et al. [23-24] suggest that the increase of tortuosity with hydration is indicative of both the filling of pores and the decreasing connectivity of the pore structure in an alkali-activated slag system because slag pastes have a very disconnected pore structure. Combined with the former reports, it determines that tortuosity could be used as a critical measure of mechanical

Preprints (www.preprints.org) | NOT PEER-REVIEWED | Posted: 7 June 2023 doi:10.20944/preprints202306.0562.v1

properties. Because the coexistence of C-S-H and (N, C)-A–S–H mainly derives from slag and amorphous geopolymer, more disconnected pore and cross-link network structure reconstruct, prompting more irregular and tortuous structure of the binder. It is in agreement with the investigation of Collins [25] that the capillary pores within alkali-activated slag concrete have variable cross-section shape, surface roughness, tortuosity, and random meeting and divergence with adjacent pores.

It is the replacement of FA with 10 wt% SF that diminishes the porosity (13.47%) and improves the tortuosity (116.9) obviously as shown in **Table 2**, more as-formed $Si(OH)_4$ hydrolyzed from the incorporating SF into the alkali-activated slag/FA system, boost and extend the ≡Si-O-Si≡ chains due to the polycondensation or crosslinking, and promote the formation of electronegative geopolymerical cages with three-dimensional networks, the Ca^{2+} is easily attracted and trapped into the cages for equilibrium charge.

3.3. Mechanical Properties of specimens subjected to freeze-thaw cycles

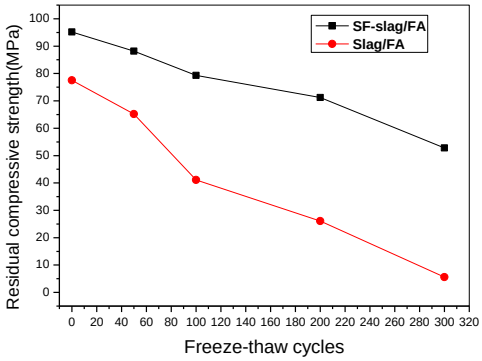

Figure 5. Compressive strengths of binders.

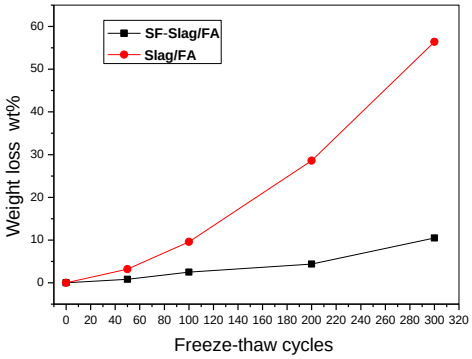

Figure 6. Weight losses of binders.

The residual compressive strength and weight loss of specimens subjected to freeze-thawing cycles are shown in **Figure 5-6**, it presents continuous decline with the increasing cycle, but the residual compressive strength of SF-containing specimen drops from 95.2 to 52.8 after 300 cycles (decreased by 44.5%), that of the specimen without SF decreases by 92.8%. However, the weight loss of specimen without SF attains 56.4% while that of SF-containing specimen is only 10.5 wt% after 300 cycles. It demonstrates that trinary SF/slag/FA binder holds higher frost resistance than binary specimens without SF.

Combining with the results of pore size distribution, due to the lower porosity and higher pore volume with pore diameter<20 nm after incorporating SF, which favor a lower absorption of free water, the expansion stress derived from the freeze-thawing of water involved in matrix decreases and suspends the deterioration of specimen. Because the

 doi:10.20944/preprints202306.0562.v1

addition of SF in Portland cement causes a significant slowdown of capillary water uptake and a higher frost resistance [26,27]. Sun et al. [28] also suggest that freeze–thawing durability of FA-based alkali-activated mortars is superior to that of Portland cement mortars. It implies that SF holds great potential to improve the frost resistance of inorganic siliceous binders to some extent.

During the freezing-thawing cycles, (i) freezing increases hydraulic water pressure and augments volume; (b) ice crystals are formed within the capillary pores; and (iii) in the liquid state, the lack of acid-base equilibrium results in osmotic pressure [19, 29]. The doped SF could transform into reactive $Si(OH)_4$ under alkaline activation, which could crosslink the (N, C)-A–S–H and facilitates the chain propagation, leading to an increase in the pore volume with pore diameter<20 nm, as well as the reduced free water within the binder. Li et al.[30] propose the nano-nucleation effect, nano-filling effect, crack arrest effect and mechanical interlocking effect of modified MWCNTs make geopolymer mortars denser, decreasing the percentage of the capillary pore. Chen et al. [31] also assert that the as-formed C–S–H gel furtherly fills the capillary pores and diminishes the frost attack. Generally, the doped SF facilitates the propagation of the (N, C)-A–S–H chains within the trinary SF/slag/FA binder, improving its freezing-thawing resistance effectively.

3.4. XRD analysis

The XRD spectra are shown in Figure 7, and the coexistence of mullite, quartz, tobermorite, and hydrated calcium silicate is displayed in the samples. There is a hump due to the amorphous silicates involved in the specimen, and the hump area of the SF-containing specimen is larger than that of the specimen without SF ($A_2>A_1$), corresponding to the increased content of amorphous binder to some extent, matching higher mechanical properties. The amorphous silicates mainly consist of the (N, C)-A–S–H and the C-S-H gels, which drive from the reconstructing of the activated $[Si(OH)_4]$ and $[Al(OH)_4]^-$, as well as the active C-H-S from the slag. Enhanced crosslinking or chain propagation is crucial for obtaining excellent mechanical strength.

Meanwhile, the mullite and quartz belong to inert substances derived from FA, which are inert to participate in the geopolymerization. However, the slightly characteristic peaks of tobermorite are detected after the substitution of 10 wt% SF for 10 wt% FA, it is demonstrated that active silicon dioxide favors the formation of tobermorite to some extent. Combined with that excessive Ca^{2+} is detrimental to flexural strength, while the SF-containing geopolymer is beneficial to improve flexural strength. Therefore, the doped SF favors the chain propagation of the amorphous silicates of (N, C)-A–S–H.

Preprints (www.preprints.org) | NOT PEER-REVIEWED | Posted: 7 June 2023 doi:10.20944/preprints202306.0562.v1

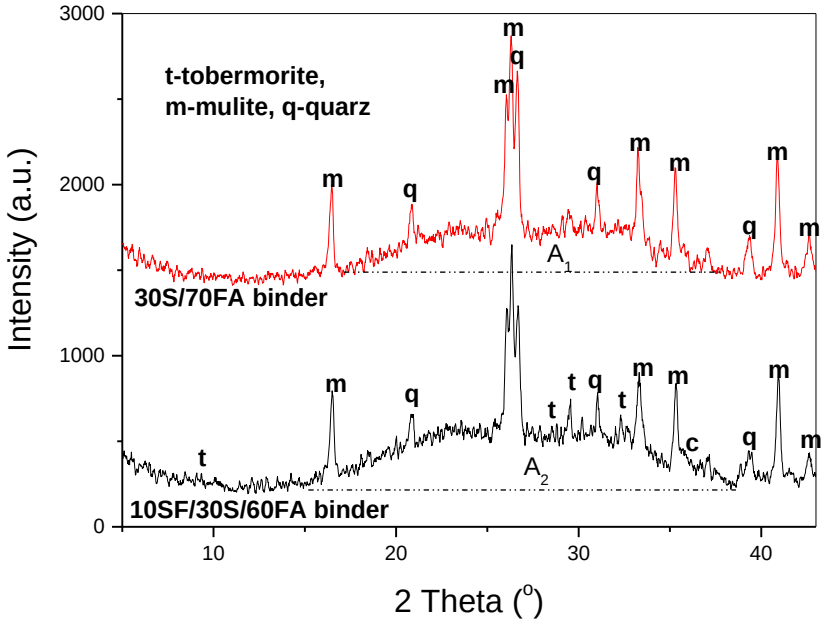

Figure 7. XRD of samples.

3.5. DSC

The heat flow curves of samples are shown in Figure 8, continuous heat absorption occurs on the samples. There is a clear endothermic peak during 50-200℃ predominantly, it is assigned to the free water evaporation involved in the micro-voids and dehydration of the calcium-rich silicate gels, it shifts slightly to a higher temperature with the increasing content of slag. Combined with the results of MIP, it deduces that the smaller median pore diameter facilitates the higher evaporation temperature. Zhang et al. [10] suggest that the resin has a filling effect and improves the evaporation temperature in alkali-activated metakaolin/slag-based geopolymer.

Meanwhile, there is no endothermic peak during 300-500℃, indicating that the calcium hydroxide does not exist in the sample. On the other hand, the area of the endothermic peak increases, and a slight exothermic peak appears with the increase of slag amount, that of the alkali-activated slag/FA (slag: FA=40:60) specimen presents the maximum area and an obvious exothermic peak at 861°C, which is attributed to the decarboxylation of calcite [32], and the temperature of endothermal valley shifts to the higher temperature of 145°C, due to the increased C-S-H content between the reactive calcium and silicate.

However, the area of the endothermic peak between 100-200°C decreases for the 10 wt% SF-containing samples. Due to the enhanced crosslinking or the propagation of the (N, C)-A–S–H chains, which could combine the Si-OH in $Si(OH)_4$ monomer, and also make the Ca^{2+} in C-S-H transforms into (N, C)-A–S–H chains as charge balancing of the negative ≡Si-O-Si≡ chains. Meanwhile, the peak at 861°C is mainly assigned to the decomposition of calcium carbonate, the slag-rich sample generates some calcium carbonate derived from the reactive CaO with air CO_2, and partial $Ca(OH)_2$ reacts with the CO_2 at the beginning stage to some extent, especially for the sample (slag: FA=40:60). But it disappears for the trinary SF/slag/FA binder, it indirectly indicating that the doped SF facilitates the Ca^{2+} participate in the formation of (N, C)-A–S–H chains, rather than the C-S-H, leading to enhanced freezing-thawing resistance. Generally, the doped SF provides the Si-rich sol system derived from the reactive $Si(OH)_4$, and the Ca^{2+} in slag is preferred crosslink with ≡Si-O-Si≡ chains to form the C-S-H, the as-formed (N, C)-A–S–H chains hold higher freezing-thawing resistance than C-S-H.

Preprints (www.preprints.org) | NOT PEER-REVIEWED | Posted: 7 June 2023 doi:10.20944/preprints202306.0562.v1

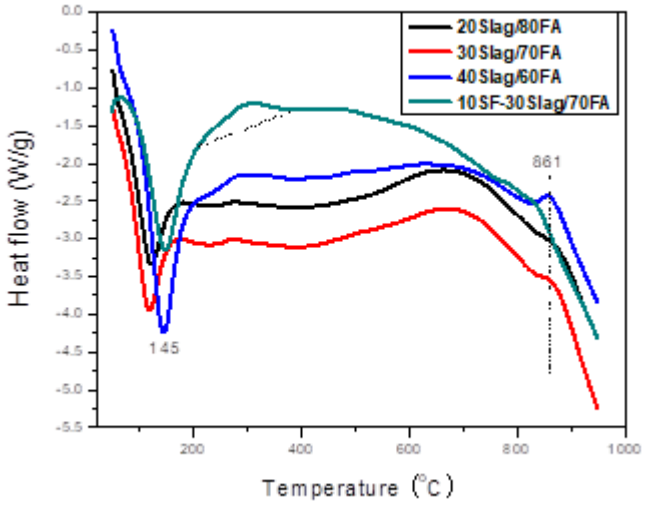

Figure 8. Heat flow curves of samples.

3.6. Morphology and Microstructure

The morphological fracture surface of the pastes after 28d-curing is presented as a series of electron micrographs with amplification of 5000× in **Figure 9**a-d, the FA has been partially activated with spherical particles in Figure 9a, displaying the coexistence of the amorphous geopolymer gels. The C-S-H and (N, C)-A–S–H chains are amorphous silicate with irregular shapes, but the C-S-H possesses a shorter chain and angular texture, while the (N, C)-A–S–H chains hold the crosslinking network structure. Partially unreacted spherical FA particles are observed, which gradually disappear with the increasing content of slag, presenting smooth and compact surface due to the as-formed C-S-H and (N, C)-A–S–H chain gels as shown in Figure 9c.

However, compared with the fracture surface of the SF-containing sample as shown in Figure 7d, the amorphous silicates exhibit a smooth and uniform surface, spherical FA particles almost disappear and compact structures are observed, which might be attributed to the enhanced geopolymerization by doping SF, leading to the more network structures, which save as silicon-aluminate cages for adsorbing Ca^{2+} and $[AlO_4]^{5-}$, thus inhibiting the C-S-H from growing effectively, corresponding to higher mechanical performance and freezing-thawing resistance. It determines that doped SF plays an important role in microstructure densification by extending the (N, C)-A–S–H chains.

Preprints (www.preprints.org) | NOT PEER-REVIEWED | Posted: 7 June 2023 doi:10.20944/preprints202306.0562.v1

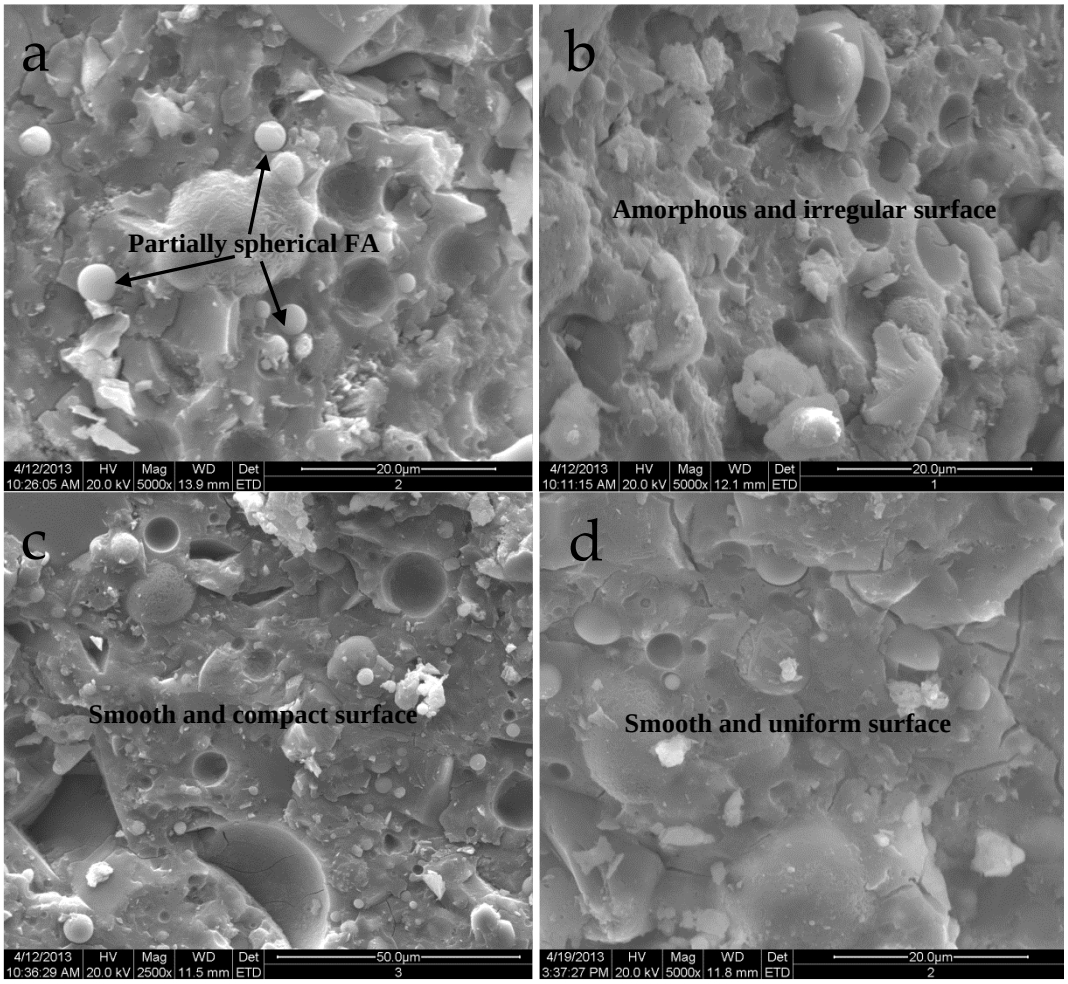

Figure 9. SEM photos of alkali-activated geopolymer paste after 28d-curing at RT (a) incorporating 20 wt% slags into FA, (b) incorporating 30 wt% slags into FA, (c) incorporating 40 wt% slags into FA, (d) incorporating 30 wt% slags and 10 wt% SF into FA.

Preprints (www.preprints.org) | NOT PEER-REVIEWED | Posted: 7 June 2023 doi:10.20944/preprints202306.0562.v1

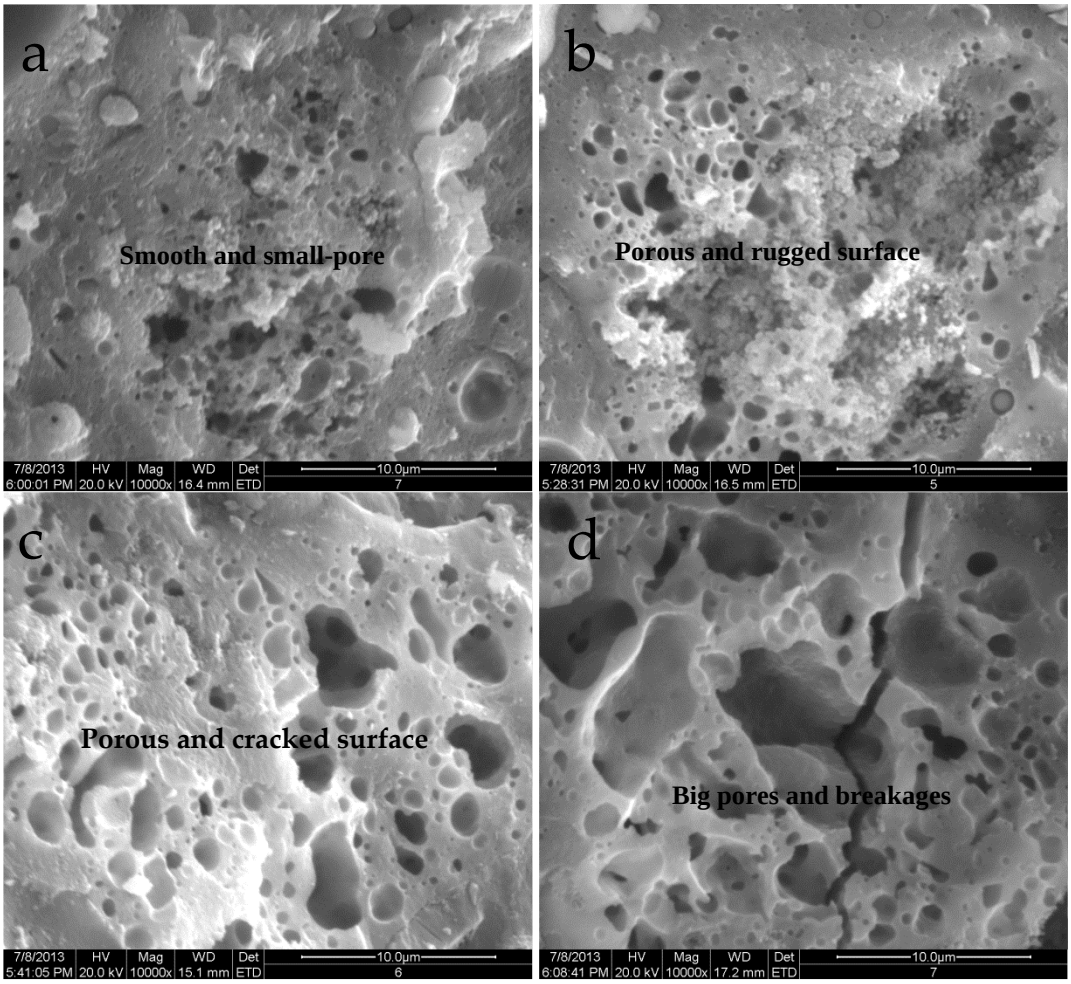

Figure 10. SEM photos of alkali-activated geopolymer paste after freeze-thaw cycles.(a) incorporating 30 wt% slag and 10 wt% SF into FA after 50 cycles, (b) incorporating 30 wt% slag into FA after 50 cycles, (c) incorporating 30 wt% slag and 10 wt% SF into FA after 125 cycles, (d) incorporating 30 wt% slag into FA after 125 cycles.

Morphologies of specimens after freeze-thawing cycles are presented as a series of electron micrographs with an amplification of 10000× in **Figure 10**a-d. The porous and rugged fracture surface is observed for the specimen without SF after freeze-thawing cycles as shown in **Figure 10**b and **Figure 10**d, compared with the smooth and small-pore fracture in **Figure 10**a and **Figure 10**c. Meanwhile, the trinary SF/slag/FA binder also presents the gradual deterioration with the increasing freezing-thawing resistance, evidenced by the porous and cracked surface. However, the binary slag/FA binder exhibits even worse deterioration, the big pores and breakages are shown in **Figure 10**d.

It demonstrates that the compact micro-structures of the trinary SF/slag/FA binder inhibit the deterioration during freeze-thawing cycles, combining with the results of MIP. The higher pore volume of larger pores holds a stronger capacity for absorbing free water and favors the greater expansion stress from frost attack, which facilitates the structural damage predominantly. On the other hand, combined with the XRD results, the formation and growth of the amorphous (N, C)-A–S–H gels prompt the compact with higher anti-freezing performance. Behfarnia et al. [33] also assert that nano-SiO_2 particles recover the particle packing density of the concrete and improve the microstructure as nano-filler, leading to considerable improvement in frost resistance.

Preprints (www.preprints.org) | NOT PEER-REVIEWED | Posted: 7 June 2023 doi:10.20944/preprints202306.0562.v1

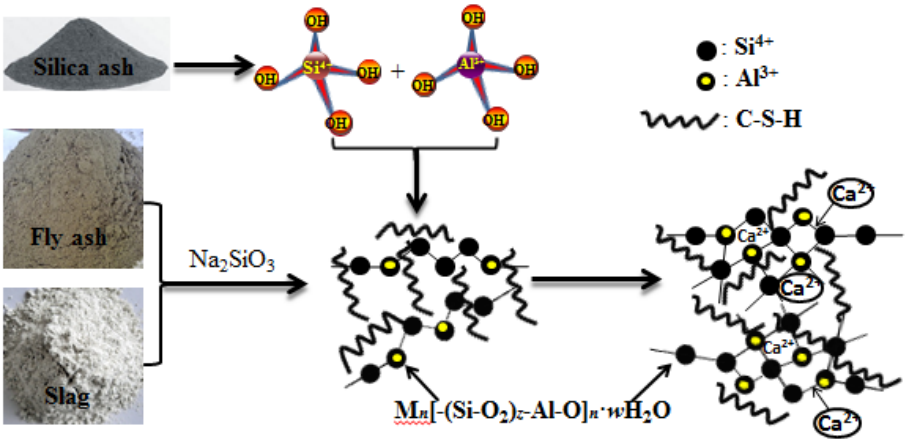

Figure 11. Schematic diagram of the reaction mechanism.

In conclusion, the slag and FA are depolymerized into $[Si(OH)_4]$ and $[Al(OH)_4]^-$ reactive under the Na_2SiO_3 activation, the Na_2SiO_3 inherently hydrolyze into ≡Si-O-Si≡ chains provide the prerequisites of the subsequent chain propagation. There is competition between the formation of C-S-H and short-chain amorphous silicate $M_n[-(Si-O_2)z-Al-O]_n \cdot wH_2O$ gels, which stack disorderly and hold a higher porosity and present a non-uniform microstructure from SEM. When incorporating the SF in the alkali-activated slag/FA system, it transforms into activated silica tetrahedra $[Si(OH)_4]$, which promotes the propagation of (N, C)-A–S–H chains through crosslinking between short-chain silicates and $[Si(OH)_4]$, triggering the formation of cross-linked networks or cages for trapping Ca^{2+} by electrostatic interactions. Because the Ca^{2+} involved in C-S-H is easily attracted and packaged by electrostatic force due to the electronegative $[Al(OH)_4]^-$, leading to compact microstructures with a reduced porosity (13.47%), exerting higher performance during the anti-freezing-thawing cycles, as shown in Figure 11.

4. Conclusions

A simple-yet-effective solution for the utilization of industrial solid wastes is explored in this paper, and the optimum slag dosage in alkali-activated slag/FA-based geopolymer is determined. Meanwhile, the SF is employed to construct the trinary slag/FA/SF (SF: slag: FA= 10:30:60, wt%) paste through the replacement of FA with 10 wt% SF, the following conclusions are drawn.

(1) An appropriate dosage (30 wt%) of slag is necessary to attain alkali-activated slag/FA geopolymer paste with excellent mechanical performance, and the incorporation of 10 wt% SF as starting materials is an effective approach to further alleviate its inherent fragility, evidenced by the compressive and flexural strength reached 95.2 and 3.2 MPa, respectively.

(2) Incorporation of 10 wt% SF promotes the propagation of (N, C)-A–S–H chains rather than the formation of C-S-H, evidenced by the absent exothermic peak at about 861°C from the DSC curves, leading to the increases in the pores volume with a pore diameter<20 nm and tortuosity by MIP results, corresponding to an improved freezing-thawing resistance with the residual compressive strength of 52.8 MPa and the weight loss of 10.5% after 300 freeze-thawing cycles.

Acknowledgments: The project is supported by the Natural Science Foundation of Shaanxi Province (2021CGBX-36).

References

[1] Wang S, Liu B, Zhang Q, et al. Application of geopolymers for treatment of industrial solid waste containing heavy metals: State-of-the-art review. Journal of Cleaner Production 390 (2023) 136053.

 doi:10.20944/preprints202306.0562.v1

[2] Harmal A, Khouchani O, El-Korchi T, et al. Bioinspired brick-and-mortar geopolymer composites with ultra-high toughness. Cement and Concrete Composites 137 (2023) 104944.
[3] Peng X, Li H, Hu Y. Preparation of metakaolin-fly ash cenosphere based geopolymer matrices for passive fire protection. Journal of Materials Research and Technology 23 (2023) 604-610.
[4] Raut A, Murmu A, Alomayri T. Physico-Mechanical and thermal behavior of prolong heat Cured geopolymer blocks. Construction and Building Materials 370 (2023) 130309.
[5] Harmal A, Khouchani O, El-Korchi T, et al. Bioinspired brick-and-mortar geopolymer composites with ultra-high toughness. Cement and Concrete Composites, 137 (2023) 104944.
[6] Oh J, Monteiro P, Jun S, Choi S, Clark SM. The evolution of strength and crystalline phases for alkali-activated ground blast furnace slag and fly ash-based geopolymers. Cement Concrete Res 2010;40 :189–196.
[7] Chithiraputhiran S, Neithalath N. Isothermal reaction kinetics and temperature dependence of alkali activation of slag, fly ash and their blends. Construction and Building Materials 2013; 45:233–242.
[8] Ismail I, Bernal S, Provis J, et al. Microstructural changes in alkali activated fly ash/slag geopolymers with sulfate exposure. Mater Struct 2013; 46:361–373.
[9] Chi M, Huang R. Binding mechanism and properties of alkali-activated fly ash/slag mortars. Construction and Building Materials 2013; 40:291–298.
[10] Zhang Y, Wang Y, Xu D, et al. Mechanical performance and hydration mechanism of geopolymer composite reinforced by resin. Mat Sci Eng A-Struct 2010;527:6574–6580.
[11] Zhang Y, Li S, Wang Y, et al. Microstructural and strength evolutions of geopolymer composite reinforced by resin exposed to elevated temperature. J Non-Cryst Solid 2012;358: 620–624.
[12] Yan S, Pan D, Dan J, et al. Calcium carbide residue and Glauber's salt as composite activators for fly ash-based geopolymer. Cement and Concrete Composites, 140 (2023) 105081.
[13] Yang J, Bai H, He X, et al. Performances and microstructure of one-part fly ash geopolymer activated by calcium carbide slag and sodium metasilicate powder. Construction and Building Materials, 367 (2023) 130303.
[14] Wang H, Zhao X, Gao H, et al. The effects of salt-loss soda residue and oxalate acid on property and structure of fly ash-based geopolymer. Construction and Building Materials, 366 (2023) 130214.
[15] El-Mir A, Hwalla J, El-Hassan H, et al. Valorization of waste perlite powder in geopolymer composites. Construction and Building Materials 368 (2023) 130491.
[16] Susan A. Bernal, Erich D. Rodriguez, Ruby Mejia de Gutierrez, John L. Provis, Silvio Delvasto. Activation of metakaolin/slag blends using alkaline solutions based on chemically modified silica fume and rice husk ash. Waste Biomass Valor 2012; 3:99–108.
[17] Garcia JI, Villanueva VM, Gorokhovsky AV, et al. Characteristics of a NaOH-activated blast furnace slag blended with a fine particle silica waste. J Am Ceram Soc 2002; 85 (7) :1788–92.
[18] Maheepala M, Nasvi M, Robert D, et al. A comprehensive review on geotechnical properties of alkali activated binder treated expansive soil. Journal of Cleaner Production 363 (2022) 132488.
[19] Zhang H, Kumar Sarker P, Xiao L, et al. Durability of low-carbon geopolymer mortar: Different responses to cryogenic attack caused by water content and freeze-thaw mediums. Cement and Concrete Composites 139 (2023) 105065.
[20] Jiao Z, Li X, Yu Q. Effect of curing conditions on freeze-thaw resistance of geopolymer mortars containing various calcium resources. Construction and Building Materials 313 (2021) 125507.
[21] Mardani-Aghabaglou A, Sezer GI, Ramyar K. Comparison of fly ash, silica fume and metakaolin from mechanical properties and durability performance of mortar mixtures view point. Construction and Building Materials 2014; 70:17–25.
[22] Puligill S, Mondal P. Role of slag in microstructural development and hardening of fly ash-slag geopolymer. Cem Concr Res 2013;43:70–80.
[23] Provis J, Myers R, White C, et al. X-ray microtomography shows pore structure and tortuosity in alkali-activated binders. Cem Concr Res 2012;42:855–864.
[24] Song S, Sohn D, H. M. Jennings, T. O. Mason. Hydration of alkali-activated ground granulated blast furnace slag. J Mater Sci 2000; 35: 249– 257.
[25] Collins F, Sanjayan J. Unsaturated Capillary Flow within alkali activated slag concrete. J Mater Civ Eng 2008;20:565-570.
[26] Ma H, Yu H, Sun W. Freezing–thawing durability and its improvement of high strength shrinkage compensation concrete with high volume mineral admixtures. Construction and Building Materials 2013;39:124–128.
[27] Garbalinska H, Wygocka A. Microstructure modification of cement mortars: Effect on capillarity and frost-resistance. Construction and Building Materials 2014;51:258–266.
[28] Sun P, Wu H. Chemical and freeze–thaw resistance of fly ash-based inorganic mortars. Fuel 2013;111:740–745.
[29] Abadel A, Alghamdi H. Effect of high volume tile ceramic wastes on resistance of geopolymer mortars to abrasion and freezing-thawing cycles: Experimental and deep learning modelling. Ceramics International 49 (2023) 15065–15081.
[30] Li F, Chen D, Lu Y, et al. Influence of mixed fbers on fly ash based geopolymer resistance against freeze-thaw cycles. Journal of Non-Crystalline Solids 584 (2022) 121517.
[31] Chen C, Lu C, Lu C, et al. Synergetic effect of fly ash and ground-granulated blast slag on improving the chloride permeability and freeze–thaw resistance of recycled aggregate concrete. Construction and Building Materials 365 (2023) 130015.
[32] Rashad A M. An investigation on very high volume slag pastes subjected to elevated temperatures. Construction and Building Materials 2015; 74:249–258.

 doi:10.20944/preprints202306.0562.v1

[33] Behfarnia K, Salemi N. The effects of nano-silica and nano-alumina on frost resistance of normal concrete. Construction and Building Materials 2013;48:580–584.